A New Procedure for Calculating Contact Stresses in Gear Teeth

Paisan Somprakit and Ronald L. Huston
University of Cincinnati
Cincinnati, Ohio

April 1991

NASA
National Aeronautics and
Space Administration

US ARMY
AVIATION
SYSTEMS COMMAND
AVIATION R&T ACTIVITY

ABSTRACT

This report discusses a new and innovative numerical procedure for evaluating and monitoring contact stresses in meshing gear teeth. The procedure is intended to extend the range of applicability and to improve the accuracy, of gear contact stress analysis.

Originally proposed by Burton Paul, et al., the procedure is based upon fundamental solution from the theory of elasticity. It is an iterative numerical procedure. The method is believed to have distinct advantages over the classical Hertz method, the finite-element method (FEM), and over existing approaches with the boundary element method (BEM).

Unlike many classical contact stress analyses, friction effects and sliding are included. Slipping and sticking in the contact region are studied.

Several examples are discussed. The results are in agreement with classical results. Applications are presented for spur gears.

1. INTRODUCTION

Tooth contact stresses are not nearly as well understood as root stresses and fillet stresses, and yet contact stresses are among the most important factors in determining gear life. Contact stresses also have a significant effect upon tooth deformations and thus upon gear performance under load.

One of the reasons that gear contact stresses are not better understood is the geometry and kinetics of meshing gear teeth do not satisfy the assumption required of the direct application of established Hertzian procedures. The Hertz analysis assumes contact between frictionless cylinders. Also, since contact stresses represent stress concentrations with nonlinear behavior, accurate results are not readily obtained with standard finite element procedures. Finally, the use of other numerical procedures such as the boundary element method (BEM) are not yet fully developed so that they are easily applied with mating gear tooth surfaces.

In this report we present a new contact stress analysis procedure which is intended to produce an improved understanding of gear contact stresses. This procedure does not require the restrictive assumptions of the Hertz analysis. Specifically, with this new procedure non-cylindrical geometry can readily be accommodated and frictional effects can be included.

The approach is based upon the point load superposition method developed by Paul, et. al. [21,24,27]* and previous, unpublished work of Sisira Jayasinghe at the University of Cincinnati. The report itself is an expansion of a paper presented at the NASA sponsored Second Annual Conference on Health Monitoring for Propulsion Systems in Cincinnati (1990) [47].

Historically, contact stresses have been one of the most important, most widely studied, and yet most difficult problems in the theory of elasticity. Contact stress analysis can be traced back to the work of H. Hertz in 1881 [1,2,3] who studied the contact deformation of smooth elastic bodies pressed together by forces normal to their contacting surfaces. He proposed that the contact region could be modelled by an elastic half space loaded over an elliptical area.

Hertz's theories have formed the basis for contact stress analyses for nearly a century. However, important contributions, extensions, and applications have been developed by Ahmadi, Keer, and Mura [4]; Barber [5]; Bentall and Johnson [6]; Boussinesq [7]; Bryant and Keer [8]; Carter [9]; Cerruti [10]; Conry and Seireg [11]; Cooper [12]; Danders [13]; Dyson [14]; Gladwell [15]; Goodman [16]; Johnson [17, 18]; Kalker and Piotrowski [19]; Keer, Dunders, and Tsai [20]; Liu and Paul [21]; Lo [22]; Mindlin [23]; Paul and Hashuni [24]; Paritsky [25]; Sackfield and Hills [26]; and Singh and Paul [27]. Excellent summaries of contact stress analysis can be found in the books of Gladwell [28] and Johnson [29] and in the review article of Kalker [30].

References [31 to 44] describe recent attempts to use the finite element method (FEM) and the boundary element method (BEM) to determine contact stresses. Since

---

*Numbers in brackets refer to the References.

contact stresses form local stress concentrations, there are convergence problems with the FEM due to the large stress gradients. Many elements are needed in the contact region to obtain an accurate representation of the stress. Also, iterative procedure and nonlinear gap elements are needed to define the contact region. Alternatively, the BEM, which is useful for problems with high stress gradients, also requires an iterative procedure to determine the contact region, but it may provide more accurate results than the FEM. Unfortunately, there is relatively little BEM software, with documentation, applicable to contact analysis.

The method of this report is an iterative numerical procedure based upon fundamental solutions of the theory of elasticity. As with the BEM it employs boundary elements on the surfaces of the mating bodies, but only within the contact region itself.

The balance of the report is divided into nine parts with the following part summarizing some preliminary results useful in the sequel. The next three parts present the basic analysis. Numerical procedures are then discussed followed by some simple examples. The next part discusses application with spur gears. The final two parts contain a discussion and concluding remarks.

2. PRELIMINARY CONSIDERATIONS

Consider two elastic bodies in contact and let the contact region be divided into a mesh of elements (or cells). Let the forces transmitted across each cell be represented by a distribution of concentrated forces acting on an elastic half space. Then by using classical results from the theory of elasticity, together with the principle of superposition, the stress distribution and point displacements due to a cell loading are obtained. Finally, by superposing the results from each cell the resulting stress and displacement distributions within the contacting bodies are obtained.

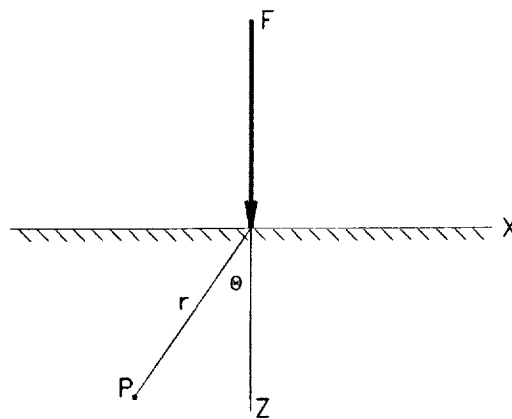To develop the analysis consider an elastic half space with a concentrated normal load as in Figure 1.

Figure 1. A Concentrated Normal Force on an Elastic Half Space

Let P be a typical point within the half space, located by the polar coordinates (r, θ) as shown. Then the radial and tangential stresses at P are [29, 45, 46]:

$$\sigma_{rr} = -\frac{2F}{\pi r} \cos \theta, \quad \sigma_{r\theta} = \sigma_{\theta\theta} = 0 \tag{1}$$

In rectangular coordinates, these stresses have the form:

$$\sigma_{xx} = -\frac{2F}{\pi} \frac{x^2 z}{(x^2+z^2)^2}, \quad \sigma_{zz} = -\frac{2F}{\pi} \frac{z^3}{(x^2+y^2)^2}, \quad \sigma_{zx} = -\frac{2F}{\pi} \frac{xz^2}{(x^2+z^2)^2} \tag{2}$$

Using the stress-strain equations and the strain-displacement equations, the displacements at a point P on the surface may be expressed as [29]:

$$u_x = -F \frac{(1-2v)(1+v)}{2E} \left(\frac{x}{|x|}\right), \quad u_z = 2F \frac{1-v^2}{\pi E} \ln|h/x| \tag{3}$$

where E and v are the elastic constant and Poisson's ratio, and where h is the distance to a reference point of zero displacement along the z-axis.

In like manner, if there is a concentrated tangential force G acting at o the stresses at P are [29]:

$$\sigma_{rr} = -\frac{2G}{\pi r} \cos \theta, \quad \sigma_{r\theta} = \sigma_{\theta\theta} = 0 \tag{4}$$

where θ is now measured from the line of action of G. In rectangular coordinates these stresses are

$$\sigma_{xx} = -\frac{2G}{\pi} \frac{x^3}{(x^2+z^2)^2}, \quad \sigma_{zz} = -\frac{2G}{\pi} \frac{xz^2}{(x^2+z^2)^2}, \quad \sigma_{zx} = -\frac{2G}{\pi} \frac{x^2 z}{(x^2+z^2)^2} \tag{5}$$

The displacement of a surface point are then

$$u_x = -2G \frac{(1-v^2)}{\pi E} \ln|x| + c, \quad u_z = G \frac{(1-2v)(1+v)}{2E} \left(\frac{x}{|x|}\right) \tag{6}$$

where c is a constant determined from a zero-displacement reference point

Next, consider an elastic half space with a distributed normal and tangential loading over a portion of the surface as depicted in Figure 2.
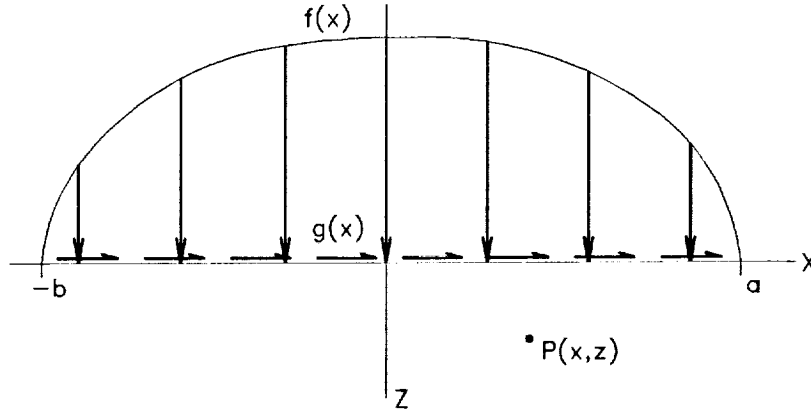
Figure 2. Elastic Half-Space with a Normal and Tangential Loading Distribution

Then the resulting stresses and displacements at a typical point P may be obtained by superposition (integration) of the foregoing results. Following the analysis of Johnson [29], the stresses at P are:

$$\sigma_{xx} = -\frac{2}{\pi}\int_{-b}^{a} \{[zf(s)(x-s)^2 + g(s)(x-s)^3]/[(x-s)^2 + z^2]^2\}ds$$

$$\sigma_{zz} = -\frac{2}{\pi}\int_{-b}^{a} \{[z^3f(s) + z^2g(s)(x-s)]/[(x-s)^2 + z^2]^2\}ds$$

$$\sigma_{xz} = -\frac{2}{\pi}\int_{-b}^{a} \{[z^2f(s)(x-s) + zg(s)(x-s)^2]/[(x-s)^2 + z^2]^2\}ds \tag{7}$$

In the manner the tangential and normal displacements of a surface point are [29]:

$$u_x = -\frac{(1-2v)(1+v)}{2E}\left[\int_{-b}^{x} f(s)ds - \int_{x}^{a} f(s)ds\right] - \frac{2(1-v^2)}{\pi E}\int_{-b}^{a} g(s)\ell n|x-s|ds + c_1$$

$$\tag{8}$$

$$u_z = -\frac{2(1-v^2)}{\pi E}\int_{-b}^{a} f(s)\ell n|x-s|ds + \frac{(1-2v)(1+v)}{2E}\left[\int_{-b}^{x} g(s)ds - \int_{x}^{a} g(s)ds\right] + c_2$$

5

where c_1 and c_2 are constants to be determined from the displacement of an arbitrary reference point.

3. APPLICATION: TRIANGULAR SHAPE LOADING DISTRIBUTION

Equations (7) and (8) may be used to determine the effects of the force distribution in the contact region. If the region is divided into a mesh of elements (or cells), then the effects of the loadings on the individual cells may be superimposed. Moreover, the general loading in contact region may be represented by the superimposed loadings on the cells. A triangular (that is, piecewise linear) loading distribution over a cell forms a convenient basis for modelling the general loading distribution.

The contribution of a triangular load on an individual cell to the stress at a typical point P may be obtained by letting f(x) and g(x) of Equations (7) and (8) have the forms:

$$f(x) - f_0(a-|x|)/a \ , \ g(x) - g_0(a-|x|)/a \ , \ |x| \ \leq \ a \qquad \qquad (9)$$

where a is the half-width of the cell whose center is at the origin, and where f_0 and g_0 are the peak triangular normal and tangential loadings as depicted in Figure 3.
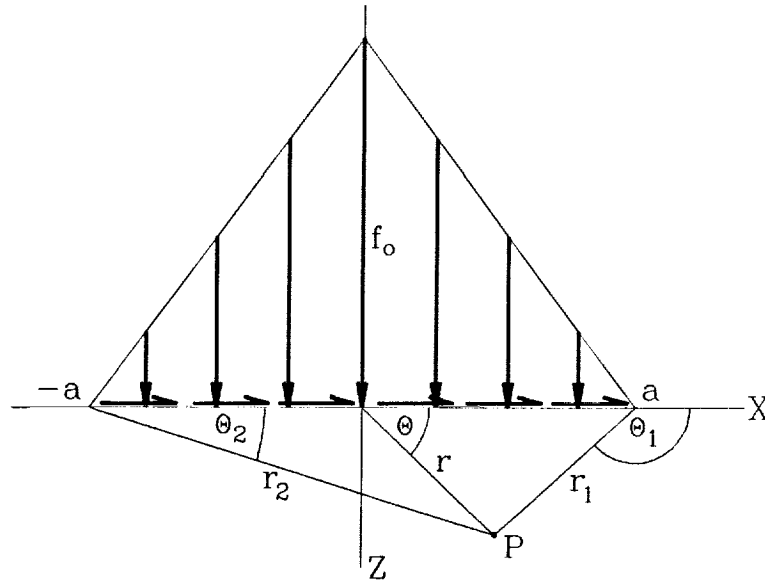

Figure 3. Triangular Normal and Tangential Loading on a Typical Cell

By substituting from Equations (9) into (7) and by performing the indicated integrations, the resulting stresses at P (see Figure 3) are [29]:

6

$$\sigma_{xx} = \frac{f_o}{\pi a}[(x-a)\theta_1 + (x+a)\theta_2 - 2x\theta + 2z\ln(r_1 r_2/r^2)]$$

$$+ \frac{g_o}{\pi a}[(2x\ln(r_1 r_2/r^2) + 2a\ln(r_2/r_1) - 3z(\theta_1 + \theta_2 - 2\theta)]$$

<div align="right">(10)</div>

$$\sigma_{zz} = \frac{f_o}{\pi a}[(x-a)\theta_1 + (x+a)\theta_2 - 2x\theta] - \frac{g_o z}{\pi a}(\theta_1 + \theta_2 - 2\theta)$$

$$\sigma_{xz} = -\frac{f_o z}{\pi a}(\theta_1 + \theta_2 - 2\theta) + \frac{g_o}{\pi a}[(x-a)\theta_1 + (x+a)\theta_2 - 2x\theta + 2z\ln(r_1 r_2 r^2)]$$

where r_1, r_2, r, θ_1, θ_2, and θ are given by (See Figure 3):

$$r_1^2 = (x-a)^2, \quad r_2^2 = (x+a)^2 + z^2, \quad r^2 = x^2 + z^2$$

<div align="right">(11)</div>

$$\tan\theta_1 = z/(x-a), \quad \tan\theta_2 = z/(x+a), \quad \tan\theta = z/x$$

Similarly, the displacements of a surface point are:

$$u_x = Ag_0[(x+a)^2\ln(x/a+1)^2 + (x-a)^2\ln(x/a-1)^2 - 2x^2\ln(x/a)^2] + Bf_0 + C_1$$

<div align="right">(12)</div>

$$u_z = Af_0[(x+a)^2\ln(x/a+1)^2 + (x-a)^2\ln(x/a-1)^2 - 2x^2\ln(x/a)^2] - Bg_0 + C_2$$

where C_1 and C_2 are constants to be determined from the displacements of a reference point and where A and B are defined as:

<div align="center">7</div>

$$A - \frac{-(1-v^2)}{2\pi EA}$$

$$B - \begin{cases} \mp \dfrac{(1-2v)(1+v)}{E} (\dfrac{a}{2}) & \text{for} \quad x \begin{smallmatrix} < \\ > \end{smallmatrix} a \\[3mm] - \dfrac{(1-2v)(1+v) \; x \; (\; a \; - \; | \; a/2 \; | \;)}{Ea} & \text{for} \quad | \; x \; | \; \leq \; a \end{cases}$$

$$(13)$$

4. MODELLING OF CONTACT FORCE DISTRIBUTION

To illustrate how these results can be superimposed in the contact region, suppose that the contact force distribution is represented by the piecewise linear distribution, as in Figure 4.
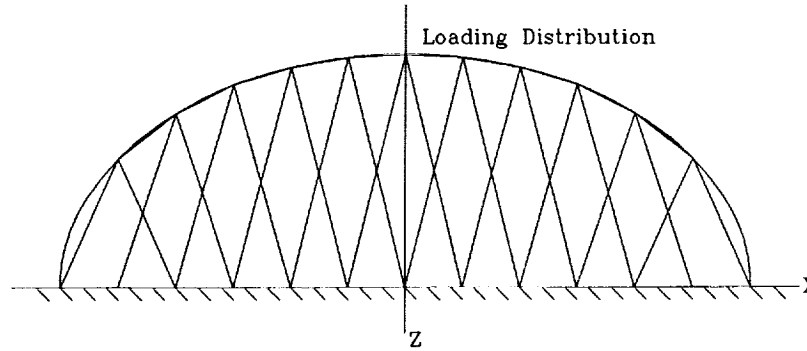
Figure 4. A Piecewise Linear Representation of a Force Distribution

Let the contact region be divided into **n** equal-width elements (or cells) as shown. Then, just as the region is discretized so also are the force and displacement distributions. Let a be the element half-width. Then the element nodal coordinates are in multiples of a. That is, the x-coordinate of node k is:

$$x_k - ka \tag{14}$$

Let u_{ix} and u_{iz} represent the tangential and normal displacements of node i due to a triangular normal load centered at node j. Then from Equations (12), u_{ix} and u_{iz} may be expressed as

8

$$u_{ix} = -\frac{(1-2v)(1+v)}{E}d_{ij}f_j \ , \qquad u_{iz} = (\frac{1-v^2}{E})c_{ij}f_j \qquad (15)$$

$$c_{ij} = \begin{cases} -\dfrac{a}{2\pi}[(k+1)^2\ln(k+1)^2+(k-1)^2\ln(k-1)^2-2k^2\ln k^2] & |k|>1 \\[2mm] 0 & k=0 \\[2mm] -\dfrac{2a}{\pi}\ell n4 & k=\pm1 \end{cases} \qquad (16)$$

$$d_{ij} = \begin{cases} a/2, & k>0 \\ -a/2, & k<0 \\ 0, & k=0 \end{cases}$$

where k is defined as:

$$k = i - j \qquad (17)$$

Equation (15) may be used to obtain the displacements at node i due to a set of superposed triangular load distributions centered at each of the nodes. In this case the terms $c_{ij}f_i$ and $d_{ij}f_j$ are interpreted as sums over j.

Finally, if there is a horizontal or tangential loading, an analogous analysis leads to displacements at node i as:

$$u_{ix} = (\frac{1-v^2}{E})c_{ij}g_j \ , \quad u_{iz} = \frac{(1-2v)(1+v)}{E}d_{ij}g_j \qquad (18)$$

where the coefficients c_{ij} and d_{ij} are the same as those of Equations (16) and where there is a sum on j from 1 to n.

The displacements of Equations (15) and (18) are measured relating to a convenient reference point, say the origin of the coordinate axes.

5. CONTACT ANALYSIS

Equation (15) and (18) may be used to develop an iterative procedure for obtaining a detailed and comprehensive analysis of contact stresses and deformations.
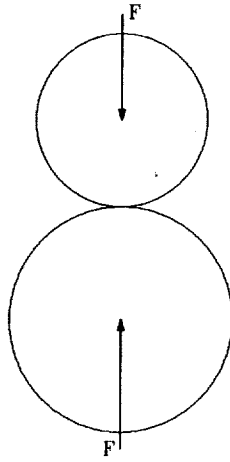
Figure 5. Two Elastic Cylinders Being Pressed Together

To illustrate this consider two cylinders pressed together as in Figure 5. As the cylinders are brought together they initially have line contact. Then as they are pressed tighter the line contact develops into a contact strip.

Figure 6 depicts the contact region after a finite deformation. The solid curves represent the deformed surface profiles, and the dashed curves represent the undeformed, or original profiles.

Figure 6. Contact Region of Deformed Cylinders

10

Consider two points Q_1 and Q_2 relatively distant from the contact region. Then during the compression Q_1 and Q_2 move toward the contact region and toward each other through the displacements d_{1z} and d_{2z} respectively.

Consider two typical matching surface points P_1 and P_2 separated by a distance $h(x)$. Then as the deformation proceeds, P_1 and P_2 simultaneously move toward each other and deform inward into their respective cylinders. Let U_{1z} and U_{2z} (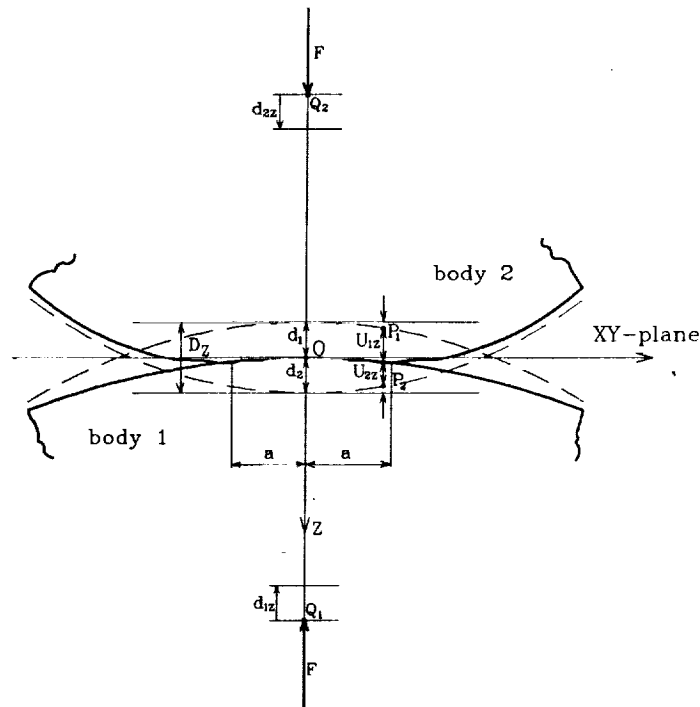measured as positive <u>into</u> the respective cylinders) represent the z-axis displacements of P_1 and P_2 toward Q_1 and Q_2. Then if P_1 and P_2 come into contact, we have

$$U_{1z} + U_{2z} + h(x) - d_{1z} + d_{2z} - D_z \tag{19}$$

where D_z is the global compressive displacement of the cylinders. If P_1 and P_2 are outside the contact region we have

$$U_{1z} + U_{2z} + h(x) > D_z \tag{20}$$

Equations (19) and (20) can be used to determine the extent of the contact region.

If there is no relative **horizontal** displacement of P_1 and P_2, we have the **no-slip** condition

$$U_{1x} - U_{2x} \tag{21}$$

When the cylinders are subjected to tangential loading in addition to the normal loading, the deformation geometry depends upon the relative magnitudes of the normal and tangential loads. The tangential loading causes on asymmetric deformation pattern. This asymmetry, or distortion is limited by the friction coefficient so that alternatively sliding occurs.

Figure 7 depicts the cylinders in contact with tangential loading. As before P_1 and P_2 are matching surface points at the initiation of contact. When the tangential load G is applied the distant points Q_1 and Q_2 have "rigid body" displacements d_{1x} and d_{2x} relative to O. If the displacements of P_1 and P_2 relative to O are denoted by S_{1x} and S_{2x}, the "slip" S_x between P_1 and P_2 may be defined as:

$$S_x - S_{1x} - S_{2x} - (U_{1x} - d_{1x}) - (U_{2x} - d_{2x}) - (U_{1x} - U_{2x}) - (d_{1x} - d_{2x}) \tag{22}$$

11

Figure 7. Contact Region with Tangential Loading

If P_1 and P_2 are in the non-slip ("stick") region s_x is zero, and then

$$U_{1x} - U_{2x} - d_{1x} - d_{2x} - D_x \tag{23}$$

where D_x is the global tangential displacement of the cylinders.

6. NUMERICAL PROCEDURES

Equations (15) and (18), together with the constraint equations of the foregoing part, may be used to determine the modal normal and tangential forces f_i and g_i. A difficulty which arises however, is that the extent of the contact region is not known a-priori. Hence, an iterative procedure needs to be developed which will determine the contact region as well as the nodal forces.

For the development of this procedure, it is convenient to superimpose Equations (15) and (18) and express them in the form:

$$u_{0x} - u_{ix} - \frac{(1-2v)(1+v)}{E} \hat{d}_{ij}f_j - \frac{1-v}{E} \hat{c}_{ij}g_j \tag{24}$$

and

$$u_{0z} - u_{iz} = - \frac{(1-2v)(1+v)}{E} \hat{d}_{ij}g_j - \frac{(1-v^2)}{E}\hat{c}_{ij}f_j \qquad (25)$$

where $\hat{c}_{oj}$ and $\hat{d}_{ij}$ are defined as

$$\hat{c}_{ij} = c_{ij} - c_{oj} \quad \text{and} \quad \hat{d}_{ij} = d_{ij} - d_{oj} \qquad (26)$$

where $\hat{c}_{0j}$ and d_{0j} are influence coefficients of the origin [see Equation (16) and (17).] Then by substituting form Equations (24) and (25) into Equation (20) we have

$$\lambda_1 \hat{c}_{ij}f_j + \lambda_2 \hat{d}_{ij}g_j = -b_i \qquad\qquad i,j = 0,...,\pm n \qquad (27)$$

where

$$\lambda_1 = \frac{(1-v_1^2)}{E_1} + \frac{(1-v_2^2)}{E_2} \quad \text{and} \quad \lambda_2 = \frac{(1-2v_1)(1+v_1)}{E_1} - \frac{(1-2v_2)(1+v_2)}{E_2} \qquad (28)$$

with E_1, $_1$, E_2, and $_2$ being the elastic constants of Bodies 1 and 2.

Similarly, for those nodes in the stick region Equations (24) and (25) together with Equations (21) lead to

$$\lambda_3 \hat{d}_{ij}f_j - \lambda_4 \hat{c}_{ij}g_j = 0 \qquad\qquad i=1,...,m; \ j=0,...,\pm n \qquad (29)$$

$$\lambda_3 = \frac{(1-2v_1)(1+v_1)}{E_1} - \frac{(1-2v_2)(1+v_2)}{E_2} \quad \text{and} \quad \lambda_4 = \frac{(1-v_1^2)}{E_1} + \frac{(1-v_2^2)}{E_2} \qquad (30)$$

Finally, for those nodes in the slip region we have

$$g_i = \pm\mu f_i \qquad\qquad i = -n,...,p,p+m,...,n \qquad (31)$$

where the sign is chosen so that the force direction is opposite to the direction of slip.

In Equations (27), (29), and (31) there are $2n+1$ unknown f_i and $2n+1$ unknown g_i ($i = 0,...,\pm n$)--that is $4n + 2$ equation. Equations (27), (29), and (31) constitute $4n + 2$ equations. However, the system is not complete since when i is zero, Equations (27) and (29) are degenerate. Hence, two additional equations are needed. These are obtained from global force summation leading to:

13

$$F - f_i A_i \quad \text{and} \quad G - g_i A_i \tag{32}$$

where A_i is the element area associated with node i.

The numerical procedure is then:

(1) Assume a contact region
(2) Divide the contact region into elements or cells
(3) Assume a stick regions within the contact region
(4) Solve Equations (27), (29), and (31) for the nodal forces
(5) Adjust the extent of the contact region by deleting nodes with negative normal forces
(6) Adjust the stick region using Equation (31)
(7) Repeat steps (1) to (6) until convergence is obtained

7. EXAMPLE SOLUTIONS

To illustrate the efficacy of the method we first considered two frictionless, steel cylinders pressed together with a force of 1000 pounds per unit axial length and no tangential loading. The cylinders had radii: 100 and 150 inches; elastic modulus: 30×10^6 pounds per square inch; and Poisson ratio: 0.3. The cylinder surfaces were taken to be frictionless so that a comparison could be made with the classical Hertz solution, which assumes frictionless contact.

Table 1 shows a comparison of numerical results and the Hertz solution.

Item	Hertz Solution	Numerical Solution	Difference
Width of Contact Region (in)	0.136156	0.137287	0.83%
Maximum Normal Pressure (psi)	9351.35	9358.90	0.08%
Maximum Shear Stress (psi)	2808.05	2810.26	0.08%
Location of Maximum Shear on Z-Axis (in)	0.05310	0.05352	0.79%

Table 1. Comparison of Hertz and Numerical Solutions for Contacting Steel Cylinders Without Friction

Next to examine the effects of friction (and hence, the consequences of neglecting friction), we considered two unlubricated cylinders with radii 100 and 150 inches made of steel and aluminum respectively. Different materials were chosen to illustrate the effects of material properties on the solutions. (The Hertz solution is based upon identical material

properties of the contacting bodies.) As in the first example, the cylinders were pressed together with a normal force of 1000 pounds per unit axial length. The elastic moduli for steel and aluminum were taken as: 30×10^6 and 12×10^6 pounds per square inches and the Poisson ratios as: 0.3 and 0.33 respectively. The friction coefficient was assigned as: 0.5 to simulate the unlubricated surfaces. Table 2 shows a comparison of numerical results and the Hertz solution. Figure 8 depicts the loading distribution in the contact region.

Item	Hertz Solution	Numerical Solution	Difference
Width of Contact Region (in)	0.18896	0.18873	0.12%
Maximum Normal Pressure (psi)	6738.12	6810.89	1.08%
Maximum Shear Stress (psi)	2021.43	2081.32 (2031.28)	2.95% (0.48%)
Location of Maximum Shear on Z-Axis (in)	0.07369	0.07967 (0.06461)	8.1% (13%)

Table 2. Comparison of Hertz Solutions (Identical, Frictionless Materials) and Numerical Solutions for Contacting Steel/Aluminum Cylinders with Friction. (The numbers in parenthesis refer to the aluminum cylinder).
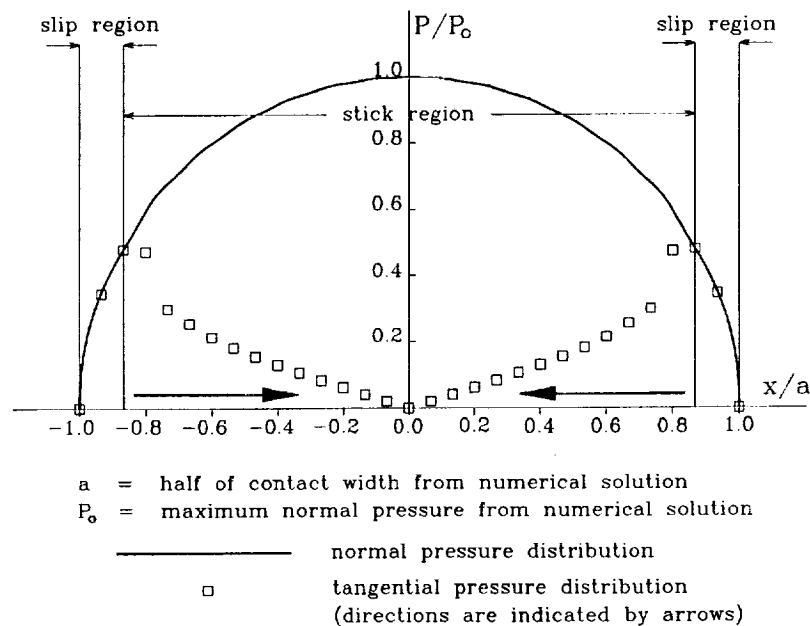

a = half of contact width from numerical solution
P_o = maximum normal pressure from numerical solution

———————— normal pressure distribution

□ tangential pressure distribution (directions are indicated by arrows)

Figure 8. Contact Region Loading Distribution for Contacting Steel/Aluminum Cylinders With Friction

Finally, to examine the effects of sliding, the steel/aluminum cylinders of the previous example were also loaded tangentially to produce sliding. Table 3 shows a comparison of the numerical results and the Hertzian solution.

Item	Hertz Solution	Numerical Solution	Difference
Width of Contact Region (in)	0.18896	0.19041	0.77%
Maximum Normal Pressure (psi)	6738.12	6737.87	0.00%
Maximum Shear Stress (psi)	2021.43	3365.39	66.4%
Location of Maximum Shear on Z-Axis (in)	0.07369	0.00	100%
Shift of Center (in)	0.00	0.01123	100%

Table 3. Comparison of Hertz Solutions (No Sliding) and Numerical Solutions for Contacting/Sliding, Steel/Aluminum Cylinders.

Figure 9 shows the normal pressure distribution obtained from the Hertz and numerical solutions. (Observe the shift in the numerical distribution due to the sliding.) Figures 10 and 11 show the shear stress distributions on the steel and aluminum cylinders for the Hertz, friction and sliding cases.
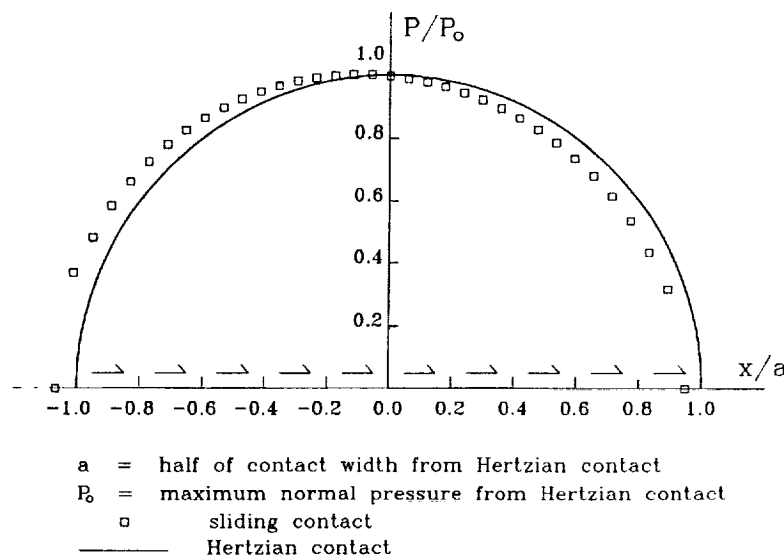

a   =   half of contact width from Hertzian contact
P_o =   maximum normal pressure from Hertzian contact
    □   sliding contact
————   Hertzian contact

Figure 9. Comparison of Hertz and Numerical Solutions for Normal Pressure for Contacting/Sliding, Steel/Aluminum Cylinders

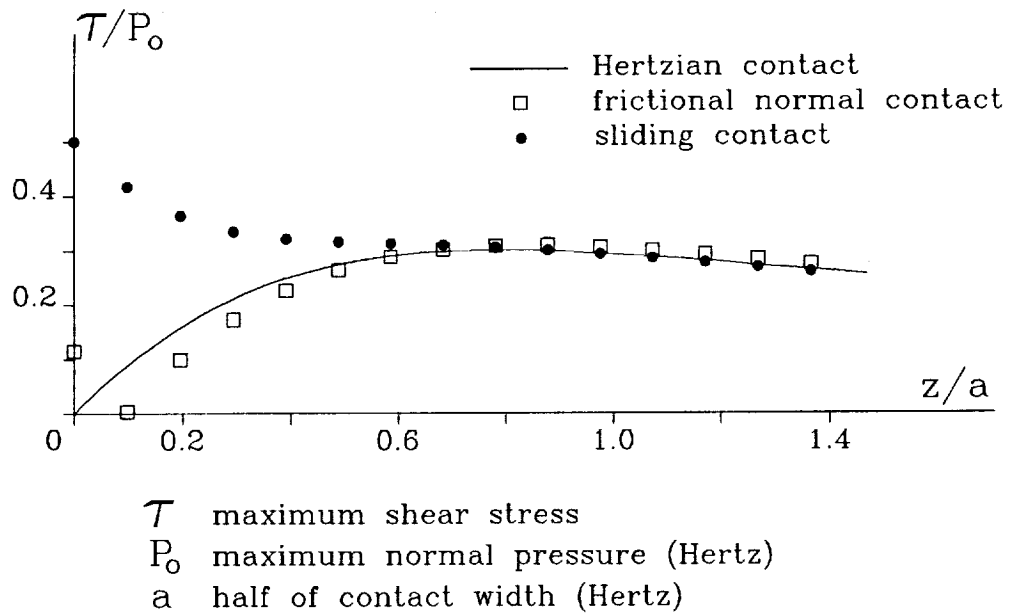T maximum shear stress
P_o maximum normal pressure (Hertz)
a half of contact width (Hertz)

Figure 10. Shear Stress Distributions on the Steel Cylinder.

T maximum shear stress
P_o maximum normal pressure (Hertz)
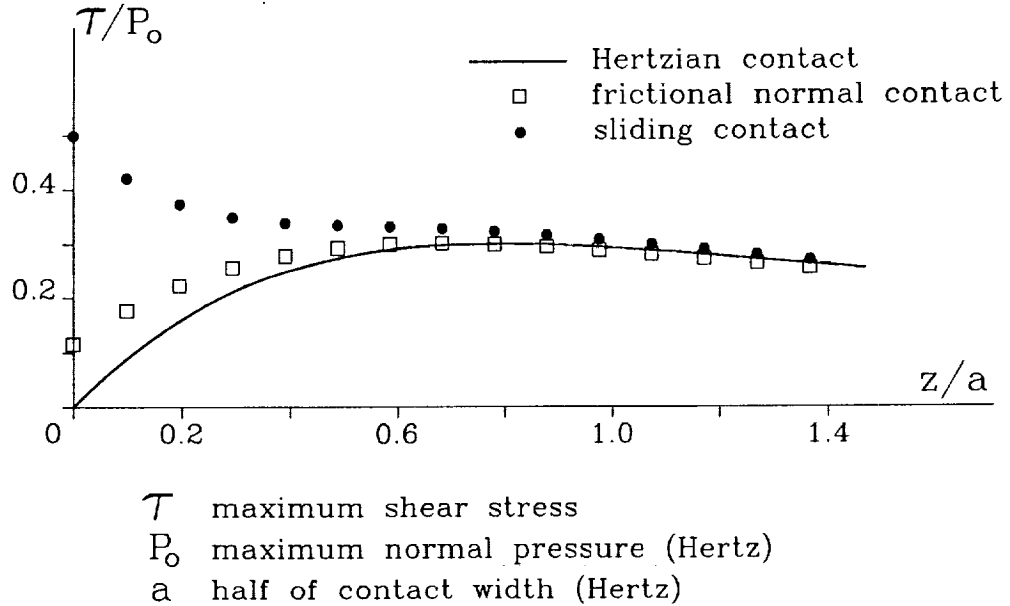a half of contact width (Hertz)

Figure 11. Shear Stress Distributions on the Aluminum Cylinder

17

8. APPLICATION WITH INVOLUTE SPUR GEARS

To study contact stresses in mating gear teeth we model the teeth as contacting cylinders as depicted in Figure 12. The radii of the cylinders depends upon the position of the contact point along the line of contact.

In Figure 12 C_1 and C_2 are the centers of the meshing gears and P is the pitch point. I_1, I_2, O_1, O_2, P, and O are points along the pressure line which is tangent to the base circles of the gears as shown. I_1 and I_2 are at the intersections of the pressure line and lines perpendicular to the pressure line passing through C_1 and C_2 respectively. O_1 and O_2 are at the intersections of the pressure line and the addenda of the gears. O is a typical contact point along the pressure line.
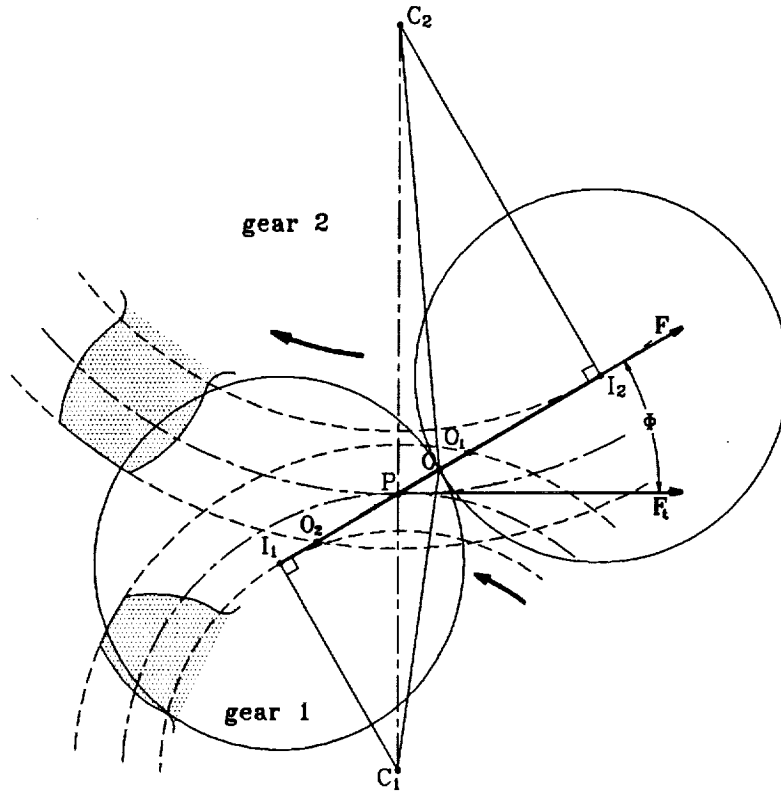

Figure 12   Modelling Mating Gear Teeth as Contacting Cylinders

With this nomenclature, if P_1 and P_2 are any two points, let P_1P_2 be the line segment connecting P_1 and P_2 and let $|\overline{P_1P_2}|$ be the length of this line segment. Then the base, pitch, and addenda circle radii are

$$r_{b1} = |\overline{C_1 I_1}| \; , \quad r_{b2} = |\overline{C_2 I_2}| \; , \quad r_{p1} = |\overline{C_1 P}| \; ,$$

$$r_{p2} = |\overline{C_2 P}| \; , \quad r_{a1} = |\overline{C_1 O_1}| \; , \quad r_{a2} = |\overline{C_2 O_2}|$$

(33)

where the subscripts 1 and 2 identify the associated gear.

Since these radii are known for a given pair of meshing gears, it is convenienct to express the tooth curvatures (and hence, the contacting cylinder curvatures) in terms of these radii. From the properties of the involute profile, the tooth radii of curvature at the contact point are simply the distances from the contact point to I_1 and I_2 respectively.
Consider the following contact positions:

1. <u>Contact at the Pitch Point</u>
In this case the radii of curvature of the mating tooth surfaces are:

$$\rho_1 = |\overline{I_1 P}| = [|\overline{C_1 P}|^2 - |\overline{C_1 I_1}|^2]^{1/2} = \sqrt{r_{p1}^2 - r_{b1}^2}$$

(34)

and

$$\rho_2 = |\overline{I_2 P}| = [|\overline{C_2 P}|^2 - |\overline{C_2 I_2}|^2]^{1/2} = \sqrt{r_{p2}^2 - r_{b2}^2}$$

(35)

where the subscripts 1 and 2 identify the associated gear.

2. <u>Contact on the Addendum Circle of Gear 1</u>
In this case the radii of curvature are:

$$\rho_1 = |\overline{I_1 O_1}| = [|\overline{C_1 O_1}|^2 - |\overline{C_1 I_1}|^2]^{1/2} = \sqrt{r_{a1}^2 - r_{b1}^2}$$

(36)

$$\rho_2 = |\overline{I_2 O_1}| = |\overline{I_1 I_2}| - |\overline{I_1 O_1}| = (r_{p1} + r_{p2})\sin\phi - \rho_1$$

(37)

where ϕ is the pressure angle.

3. <u>Contact on the Addendum Circle of Gear 2</u>
In this case the radii of curvature are:

$$\rho_2 = |\overline{I_2 O_2}| = [|\overline{C_2 O_2}|^2 - |\overline{C_2 I_2}|^2]^{1/2} = \sqrt{r_{a2}^2 - r_{b2}^2}$$

(38)

19

and

$$\rho_1 - |\overline{I_1 I_2}| - |\overline{I_2 O_2}| - (r_{p1} + r_{p2})\sin\phi - \rho_2 \qquad (39)$$

4. Contact at Other Points

Cases 2 and 3 are at the contact extremes with Case 1 being intermediate. For some other contact point, the radii of curvature will be different than these cases, but it can be calculated using the same procedures as in the above cases.

The developed numerical procedures may now be used to calculate the contact stresses on the mating teeth. To illustrate this applicaiton, consider two identical spur gears in mesh with the following properties.

Number of teeth: 18

Pitch diameter: 3.5433 in.

Face width: 0.3937 in.

Pressure angle: 20 deg.

Transmitted load: 808 lb.
(tangential)

Elastic modulus: 30×10^6 psi

Poisson ratio: 0.3

This data yields the following parameters:

Base circle radius: 1.6648 in.

Addendum circle radius: 1.9685 in.

Contact force: 860 lb.
(normal)

Contact force per
unit length: 2184 lb.

To put the results in perspective, it is informative to make comparisons between the maximum contact stresses and the maximum fillet (root) stresses, which are documented extensively in the technical literature.

Table 4. presents the results and comparisons. The tensile fillet stresses are obtained using the Lewis formula [48], the Lewis factor [49], and the stress concentration factor [50, 51]. The compressive fillet stress may be obtained using finite element methods [52]. Finally, the stresses of Table 4 are listed in psi. The maximum Von Mises stresses occur beneath the surface at depths of 0.0056 in for pitch point contact and 0.0038 in for addendum point contact. The maximum compressive contact stresses occur on the surface.

	Pitch Point Contact	Addendum Contact
Fillet Tensile Stress	N/A	46,217
Fillet Compressive Stress	N/A	55,080
Compressive Contact Stress	194,480	286,013
Von Mises Contact Stress	58,407	85,899

Table 4. Stress Results and Comparisons

9. DISCUSSION

Although these examples employ bodies with simple geometries (cylinders), the method outlined herein is not restricted to simple geometries. Indeed, there are no restrictions on the geometry so long as the contacting surfaces are continuous and geometrically smooth (that is, with continuous derivatives).

The examples demonstrate the efficacy of the method. They show that the numerical results are extremely close to those of the classical Hertz solutions, for those cases where the Hertz solution is applicable. Indeed, the stresses are virtually identical whereas there is a slight difference in the geometric results - that is, the contact region width and the location of the maximum shear stress. (The Hertz solution assumes frictionless static contact between identical materials.)

The second and third example demonstrate the significant effects of friction and sliding in contact analysis. The examples also show that the softer material has lesser stress.

In addition it is seen that friction and sliding significantly increase the shear stresses. Indeed, when there is sliding with a relatively high friction coefficient, the maximum shear stress occurs on the surface as opposed to being beneath the surface (See Figures 10 and 11).

Finally, in the examples with the gear stresses it is seen that the fillet stress is dependent upon the loading and geometry whereas the contact stress depends upon the elastic properties as well.

Regarding the method itself it is seen that it employs a double discretation: one of the contact region, the other of the force distribution. The execution of the method involves an iterative procedure to determine the extent of the contact region. In this way the method

is clearly more laborious than the classical Hertz method and even elementary finite-element methods (FEM). In exchange, however, the method is believed to provide a more accurate and comprehensive analysis than either the Hertz or FEM techniques.

The method outlined herein is developed for a two-dimensional analysis with a triangular load on the individual elements or cells. The triangular load provides for a piecewise linear representation of the contact loading. The extension to higher order load representations (for example, the use of cubic splines), and to three-dimensional analysis, is conceptually "straight-forward." Such extensions are currently being developed.

10. CONCLUSIONS

A point load superposition procedure based on the theory of elasticity has been used to study contact stresses between elastic bodies, including meshing spur gear teeth. This method is validated by comparison with results from the classical Hertz method for frictionless cylinders in contact. The following specific conclusions are reached:

1. A new method of contact stress analysis has been presented. It is a numerical method which has fewer restrictions than classical procedures.
2. The method is applicable for a broad range of geometries of the contacting bodies. The contacting bodies may have different material properties. The contacting surfaces need not be smooth. Sliding between the contacting surfaces is also permitted.
3. The accuracy of the method is demonstrated by a comparison with results from classical methods for simple cases where the classical method is applicable.
4. The established efficacy of the method justifies applications with contacting gear teeth.

REFERENCES

1. H. Hertz, "On the Contact of Elastic Solids" (in German), *J. Reine und Angwandte Mathematik*, Vol. 92, 1882, pp 156-171. (See [3] for English translation).

2. H. Hertz, "On the Contact of Rigid Elastic Solids and an Hardness" (in German), *Verhandlungen des Vereins zur Beforderung des Gewerbefleisses*, Leipzig, 1882.

3. D.E. Jones and G.A. Schott, H. Hertz, Miscellaneous Papers, *Macmillan and Co.*, London, 1896.

4. N. Ahmadi, L.M. Keer, and T. Mura, "Non-Hertzian Contact Stress Analysis-- Normal and Sliding Contact," *International Journal of Solids and Structures*, Vol. 19, 1983, p. 357.

5. J.R. Barber, "Thermoelastic Contact Problems," In: *The Mechanics of Contact Between Deformable Bodies* (de Pater and J.J. Kalker, Eds.) Delft University Press, 1975.

6. R.H. Bentall and K.L. Johnson, "Slip in the Rolling Contact of Two Dissimilar Elastic Rollers," *International Journal of Mechanical Sciences*, Vol. 9, 1967, pp 389-404.

7. J. Boussinesq, Application des Potentials a' *ℓ Etude* de *ℓ* Equilibrium et du Movement des Solids E'lastiques, Gauthier-Villars, Paris, 1885.

8. M.D. Bryant and L.M. Keer, "Rough Contact Between Elastically and Geometrically Similar Curved Bodies," *Journal of Applied Mechanics*, Vol. 49, 1982, p 545.

9. F.W. Carter, "On the Action of a Locomotive Driving Wheel," *Proceedings, Royal Society*, Vol. A112, 1926, p 151.

10. V. Cerruti, "Acc. Lincei," *Mem. Fis. Mat.*, Rome, 1882.

11. T.F. Conry and A. Seireg, "A Mathematical Programming Method for Design of Elastic Bodies in Contact, *Journal of Applied Mechanics*, Vol. 38, 1971, pp. 387-392.

12. D.H. Cooper, "Hertzian Contact-Stress Deformation Coefficients," *Journal of Applied Mechanics*, Vol. 36, 1969, pp. 296.

13. J. Dunders, "Properties of Elastic Bodies in Contact," *In: The Mechanics of Contact Between Deformable Bodies* (de Pater and J.J. Kalker, Eds.) Delft University Press, 1975, pp. 54-66.

14. A. Dyson, "Approximate Calculations of Hertzian Compressive Stresses and Contact Dimensions," *Journal of Mechanical Engineering Sciences*, Vol. 7, 1965, p 224.

15. G.M.L. Gladwell, "On Some Unbounded Contact Problems in Plane Elasticity Theory," *Journal of Applied Mechanics*, Vol. 43, 1976, pp. 263.

16. L.E. Goodman, "Contact Stress Analysis of Normally Loaded Rough Spheres," *Journal of Applied Mechanics*, Vol. 29, 1962, pp. 515-522.

17. K.L. Johnson, "The Effect of a Tangential Contact Force upon the Rolling Motion of an Elastic Sphere on a Plane," *Journal of Applied Mechanics*, Vol.

25, 1958, pp. 339.

18.   K.L. Johnson, "The Effect of Spin Upon the Rolling Motions of an Elastic Sphere on a Plane," *Journal of Applied Mechanics*, Vol. 25, 1958, pp. 332.

19.   J.J. Kalker and J. Piotrowski, "Some New Results in Rolling Contact," *Vehicle System Dynamics*, Vol. 18, 1989, pp. 223-242.

20.   L.M. Keer, J. Dunders, and K.C. Tsai, "Problems Involving Receding Contact Between a Layer and a Half-Space," *Journal of Applied Mechanics*, Vol. 39, 1972, pp. 1115.

21.   C. Liu and B. Paul, "Rolling Contact With Friction and Non-Hertzian Pressure Distribution," *Journal of Applied Mechanics*, Vol. 56, 1989, pp. 814-820.

22.   C.C. Lo, "Elastic Contact of Rough Cylinders," *International Journal of Mechanical Sciences*, Vol. 11, 1969, pp. 105.

23.   R.D. Mindlin, "Compliance of Elastic Bodies in Contact," *Journal of Applied Mechanics*, Vol. 16, 1949, pp. 259-268.

24.   B. Paul and J. Hashemi, "Contact Pressure on Closely Conforming Elastic Bodies, *Journal of Applied Mechanics*, Vol. 48, 1981, p 543.

25.   H. Poritsky, "Stresses and Deflections of Cylindrical Bodies in Contact," *Journal of Applied Mechanics*, Vol. 17, 1950, p 191.

26.   A. Sackfield and D.A. Hills, "Some Useful Results in the Classical Hertz Contact Problem," *Journal of Strain Analysis*, Vol. 18, 1983, p 101.

27.   K.P. Singh and B. Paul, "Numerical Solution of Non-Hertzian Elastic Contact Problems," *Journal of Applied Mechanics*, Vol. 41, 1974, pp. 484-490.

28.   G.M.L. Gladwell, "Contact Problems in the Classical Theory of Elasticity, Sijthoff and Noordhoff, 1980.

29.   K.L. Johnson, Contact *Mechanics*, Cambridge, London, 1985.

30.   J.J. Kalker, "A Survey of the Mechanics of Contact Between Solid Bodies," *Zeitschrift für Angwandte Mathematik und Mechanik*, Vol. 57, 1977, pp T3-T17.

31.   W.H. Chen and J.T. Yel, "Three-Dimensional Finite Element Analysis of Static and Dynamic Contact Problems With Friction, *Computers and Structures*, Vol. 35, No. 5, 1990, pp. 541-542.

32.   N. Chandrasekaraw, W.E. Haisler, and R.E. Goforth, "A Solution Method for Planar and Axisymmetric Contact Problems," *International Journal of Numerical Methods in Engineering*, Vol. 21, 1985, pp 65-88.

33.   K.J. Bathe and A. Chandary, "A Solution Method for Planar and Axisymmetric Contact Problems," *International Journal of Numerical Methods in Engineering*, Vol. 21, 1985, pp. 65-68.

34.   M.U. Rahman, R.E. Rowlands, and R.D. Cook, "An Iterative Procedure for Finite Element Stress Analysis of Frictional Contact Problems," *Computers and Structures*, Vol. 14, 1984, pp. 947-954.

35.   T.D. Sachdeva and C.V. Ramakrishnan, "A Finite Element Solution for the Two-Dimensional Elastic Contact Problems with Friction," *International Journal of Numerical Methods in Engineering*, Vol. 17, 1981, pp. 1257-1271.

36.   R.J. Gu, "Moving Finite Element Analysis for Two-Dimensional Frictionless Contact Problems, *Computers and Structures*, Vol. 33, No. 2, 1989, pp. 543-549.

37. H.S. Jing and M.-L. Liao, "An Improved Finite Element Scheme for Elastic Contact Problems with Friction," *Computers and Structures*, Vol. 35, No. 5, 1990, pp. 571-578.

38. N. Akamato and M. Nakazawa, "Finite Element Increment Contact Analysis with Various Frictional Conditions," *International Journal of Numerical Methods in Engineering*, Vol. 14, 1979, pp. 337-357.

39. M. Mazurkiewicz and W. Ostachowicz, "Theory of the Finite Element Method for Elastic Contact Problems of Solid Bodies," *Computer and Structures*, Vol. 17, 1983, pp. 51-59.

40. K.P. Oh and S.M. Rohde, "Numerical Solution of the Point Contact Problem Using the Finite Element Method," *International Journal for Numerical Methods in Engineering*, Vol. 11, 1977, pp. 1507-1578.

41. W. Ostachowicz, "Mixed Finite Element Method for Contact Problems," *Computers and Structures*, Vol. 18, 1984, pp. 937-945.

42. M.J. Abdul-Mihein, A.A. Baker, and A.P. Parker, "A Boundary Integral Equation Method for Axisymmetric Elastic Contact Problems," *Computers and Structures*, Vol. 23, 1986, pp. 787-793.

43. T. Anderson and B.G.A. Person, "The Boundary Element Method Applied to Two-Dimensional Contact Problems," *Progress in Boundary Elements*, (C.A. Brebbia, Ed.) Vol. II, Chapter 5, PentechPress, London, 1982.

44. H. Sun and R.L. Huston, "An Automatic Incrementation Technique of the Boundary Element Method for Two-Dimensional Contact Problems with Friction," *Computational Engineering with Boundary Elements* (A.H.D. Cheng, C.A. Brebbia, and S. Grilli, Eds.) Computational Mechanics Publication, Boston, 1990, pp. 19-35.

45. A.E.H. Love, *A Treatise on the Mathematical Theory of Elasticity*, 4th Edition, Cambridge University Press, 1952.

46. S.P. Timoshenko and J.N. Goodier, Theory of Elasticity, 3rd Edition, McGraw Hill, New York, 1951.

47. P. Somprakit, R.L. Huston, and J.E. Wade, "Monitoring of Contact Stresses in Advanced Propulsion Systems," Second Annual Conference on Health Monitoring for Space Propulsion Systems, Cincinnati, Ohio 1990.

48. W. Lewis, "Investigation of the Strength of Gear Teeth," Proceedings of the Engineer's Club, Philadelphia, 1983.

49. J.E. Shigley and L.D. Mitchell, Mechanical Engineering Design, Theory and Practice, MacMillan, 1975.

50. A.D. Deutschman, W.J. Michels, and C.E. Wilson, Machine Design, Theory and Practice, MacMillan, 1975.

51. T.J. Dolan and E.L. Broghamer, "A Photo-elastic study of the stresses in Gear Tooth Fillets," University of Illinois Engineering Experiment Station, Bulletin No. 335, 1942.

52. P. Somprakit, M. Pourazady, and R.L. Huston, "Effect of Fitting Parameters on Spur Gear Stresses," Proceeding of the 1989 International Power Transmission and Gearing Conference, ASME, 1989, pp 815-822.

NASA
National Aeronautics and
Space Administration

Report Documentation Page

1. Report No. NASA CR - 187094 AVSCOM TR 91-C-012	2. Government Accession No.	3. Recipient's Catalog No.

4. Title and Subtitle

A New Procedure for Calculating Contact Stresses in Gear Teeth

5. Report Date

April 1991

6. Performing Organization Code

7. Author(s)

Paisan Somprakit and Ronald L. Huston

8. Performing Organization Report No.

None

10. Work Unit No.

1L162211A47A
505-63-36

9. Performing Organization Name and Address

University of Cincinnati
Department of Mechanical, Industrial and Nuclear Engineering
Cincinnati, Ohio 45221-0072

11. Contract or Grant No.

NSG-3188

12. Sponsoring Agency Name and Address

Propulsion Directorate
U.S. Army Aviation Systems Command
Cleveland, Ohio 44135-3191
and
NASA Lewis Research Center
Cleveland, Ohio 44135-3191

13. Type of Report and Period Covered

Contractor Report
Final

14. Sponsoring Agency Code

15. Supplementary Notes

Project Manager, Fred B. Oswald, Propulsion Systems Division, NASA Lewis Research Center, (216) 433-3957.

16. Abstract

The report discusses a new and innovative numerical procedure for evaluating and monitoring contact stresses in meshing gear teeth. The procedure is intended to extend the range of applicability and to improve the accuracy, of gear contact stress analysis. Originally proposed by Burton Paul, et al., the procedure is based upon fundamental solution from the theory of elasticity. It is an iterative numerical procedure. The method is believed to have distinct advantages over the classical Hertz method, the finite-element method (FEM), and over existing approaches with the boundary element method (BEM). Unlike many classical contact stress analyses, friction effects and sliding are included. Slipping and sticking in the contact region are studied. Several examples are discussed. The results are in agreement with classical results. Applications are presented for spur gears.

17. Key Words (Suggested by Author(s))

Contact stress; Numerical methods; Elasticity;
Hertz method; Friction

18. Distribution Statement

Unclassified - Unlimited
Subject Category 37

19. Security Classif. (of the report)	20. Security Classif. (of this page)	21. No. of pages	22. Price*
Unclassified	Unclassified	26	A03

NASA FORM 1626 OCT 86 *For sale by the National Technical Information Service, Springfield, Virginia 22161